MULTIPLE-ARRAY DETECTION, ASSOCIATION AND LOCATION OF INFRASOUND AND SEISMO-ACOUSTIC EVENTS – UTILIZATION OF GROUND TRUTH INFORMATION

Stephen J. Arrowsmith[1], Il-Young Che[2], Christopher T. Hayward[3], and Brian W. Stump[3]

Los Alamos National Laboratory[1], Korea Institute of Geoscience and Mineral Resources[2] and Southern Methodist University[3]

Sponsored by the Air Force Research Laboratory and the National Nuclear Security Administration

Contract Nos. DE-AC52-06NA25396[1] and FA8718-08-C-008[2,3]

ABSTRACT

This work is intended to provide automated methodology for processing seismic and infrasound data from seismo-acoustic arrays and apply the methodology to regional networks for validation with ground truth information. In the initial year of the project automated techniques for detecting, associating and locating infrasound signals were developed. Recently, the location procedure has been cast into a Bayesian framework.

Work this year has focused on assessment of sets of robust regional infrasound signals in order to optimize the location algorithms. Quantification of the importance of model and empirical travel times, backazimuth estimation (including errors) and signal detectability have all been undertaken and are reported. Two specific studies are reported.

Infrasound from a static rocket test conducted at Promontory, Utah on11/01/2007, was observed on USArray seismographs up to a distance of 600 km. Signal durations were broadly consistent with the duration of the test, 123 s, and signal envelopes correlated with variations in thrust in some cases. The effect of adding Gaussian noise to wind profiles is investigated for the purpose of phase identification. It is shown that all observations can be predicted through the combination of simulations using different noise levels, suggesting that a probabilistic approach to phase identification is possible. These results have important implications for how atmospheric models might be utilized in source location in particular how they might be implemented into the Bayesian location framework of Modrak et al. (2010).

The deterministic dependence of infrasound propagation on the season and path environment was quantified by the analysis of more than 1,000 repetitive infrasonic ground-truth events at an active, open-pit mine in Korea over 2 years. Blast-associated infrasonic signals were analyzed from two infrasound arrays (CHNAR and ULDAR) located at similar distances of 181 and 169 km, respectively from the source but in different azimuthal directions and with different path environments. The CHNAR array is located to the NW of the source area with primarily a continental path, whereas the ULDAR is located E of the source with a path dominated by open ocean. As a result, CHNAR observations were dominated by stratospheric phases with characteristic celerities (group velocities) of 260 to 289 m/s and large seasonal variations in the travel time, whereas data from ULDAR consisted primarily of tropospheric phases with larger celerities from 322 to 361 m/s and larger daily than seasonal variation in the travel time. Ray tracing using atmospheric models incorporating daily weather balloon data that characterizes the shallow atmosphere for the 2 years of the study verifies the interpretation of these observations. Finally, experimental celerity models that included seasonal path effects were constructed from the long-term dataset. These experimental celerity models were used to constrain travel time variations in infrasonic location algorithms providing improved location estimates as illustrated with the empirical dataset.

OBJECTIVES

There are two primary objectives to our efforts in the second and third year of this contract. Each objective builds on the automatic algorithms for detection, association, and location of infrasound events developed in the first year of this project, the further development of these techniques in year two and the preliminary analysis of ground truth data in assessing atmospheric propagation models.

- **Validation and utilization of atmospheric models**. Initial efforts in this contract focused exclusively on infrasound detection, association, and location without requiring the use of atmospheric models. R&D this year has focused on how best to use prediction models (comprising the combination of atmospheric and propagation models) for enhancing source localization. In this paper we outline two different approaches: a stochastic approach and a deterministic approach, for using atmospheric specifications in event location.
- **Extended analysis of infrasound propagation effects using ground-truth data from Korea.** A primary focus in the last year has been in the careful analysis and modeling of infrasound observations associated with the ground truth data acquired in the earlier stages of the study. These data have been compared to detailed propagation path models for the Korean peninsula and provide a basis for assessing the types of empirical data that can improve location estimates based exclusively on infrasonic data and seismic and infrasonic data in combination.

RESEARCH ACCOMPLISHED

A Strategy for Enhancing the Bayesian Infrasonic Source Location (BISL) Method

The BISL framework, outlined in Modrak et al. (2010), provides a robust framework for infrasound location without requiring a prediction model. This is accomplished in part by defining a uniform prior PDF on celerity (group velocity) as follows:

$$p(v) = \begin{cases} 16.67 & 0.22 \text{ km/s} \le v \le 0.34 \text{ km/s} \\ 0 & \text{otherwise} \end{cases}.$$

This Bayesian prior term effectively takes a worst-case scenario: we have no expectation of the celerity for a given observed arrival, and can therefore only place bounds on celerity (noting that these bounds might be more restrictive if, for example, we can rule out a thermospheric return on some basis). In the absence of a reliable prediction model that is capable of predicting infrasound phases, this appears to be the best we can do for now. But is it really?

Prediction Models

Real time state-of-the-art atmospheric models, such as the Ground-to-Space (G2S) model are thought to capture the day-to-day and hourly variability in temperatures and winds at horizontal resolutions of approximately $1 \times 1°$. However, they do not attempt to resolve fine-scale atmospheric structures such as sub-grid scale gravity waves, turbulence, and wind gusts. It has been demonstrated that the combination of such atmospheric models with existing infrasound propagation models do not always reliably predict observations (e.g., Arrowsmith et al.; 2007; Evers, 2009). This is a particular problem in the zone-of-silence, a region that extends from approximately 50 to 200 km. Two factors influence this limitation: (1) the fidelity of atmospheric models, and (2) the fidelity of propagation models.

For routine infrasound location, we require a good blend of simplicity and physical thoroughness, to balance the need to be useful in operational processing and capture sufficient propagation physics. As outlined by Drob et al. (2010), the TauP method (e.g., Garcés et al., 1998; Drob et al., 2010) provides a good balance of simplicity and physical thoroughness to make it the propagation model of choice for automatic location algorithms. Other methods – such those based on Parabolic Equations or Normal Modes (see Whitaker and Norris, 2008, for a summary) – account for additional wave physics, such as diffraction effects, but are impractical for current automated techniques due to the high computational costs.

Using Prediction Models in BISL

The simple question is this: Given some smoothed realization of the atmosphere at a given place and time, how can we use that information to better constrain the group velocity? With the knowledge that we cannot

reliably predict arrivals deterministically, we need to somehow account for the unknown effects of gravity waves, turbulence, and wind gusts – as well as limitations in propagation physics – in a stochastic way. A simple way to do this is to add noise to G2S wind profiles, constrained by empirical data. We note here that Gibson et al. (2009) have used spectral models for gravity waves to perturb atmospheric models with some success, using a Time Domain Parabolic Equation method. Since our strategy is to account for multiple sources of error for event location, a simple Gaussian noise model is used here. Incorporating additional constraints such as the gravity wave spectral model of Gardner (1995) could refine this model.

Based on the fact that the dense network of seismic stations in the USArray can be used for detecting infrasound (e.g., de Groot-Hedlin et al., 2008), we can leverage this unprecedented sampling of the infrasound wavefield to test the effect of adding different levels of noise to the zonal and meridional wind components, and determine what standard deviation of noise is needed to predict the observations. A static rocket test, conducted at Promontory, Utah, at 19:00 UT on 11/01/2007 was well recorded by USArray and easy to identify on the single-channel seismic data owing to its unique source-time function of duration equal to 123 s (Figure 1).

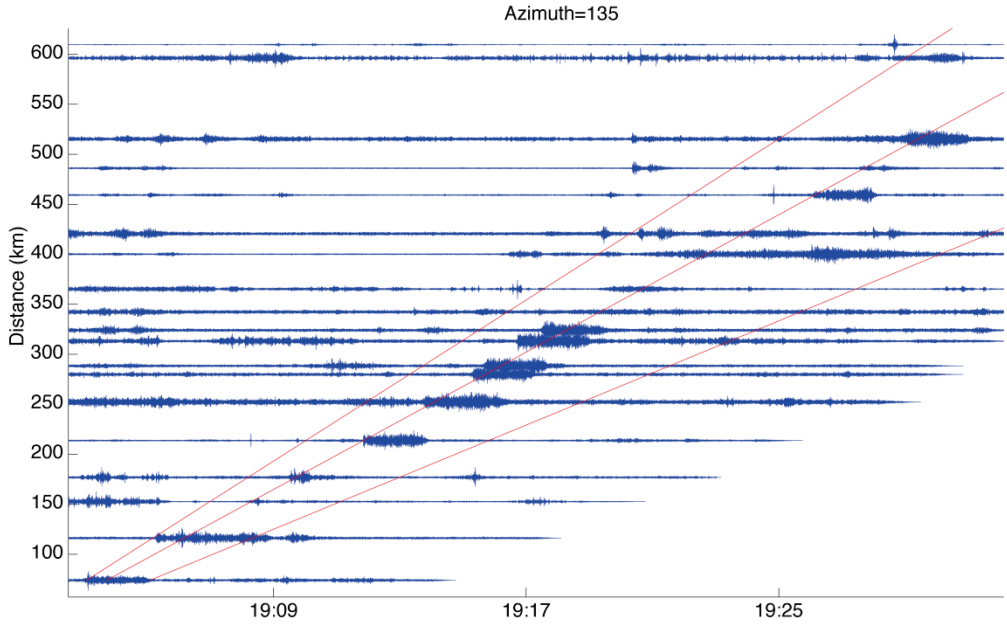

Figure 1. Record section taken along a great-circle azimuth of 135°. All stations within 20° of the great-circle azimuth are projected onto the great-circle path. Vertical component waveforms are plotted, bandpass filtered from 3-10 Hz. Red lines correspond to group velocities of 0.34 km/s, 0.29 km/s, and 0.22 km/s.

We add noise to the wind components only, since the uncertainties in temperature in the G2S model are lower (Drob et al., 2010). The implementation is simple: Mathematically, $u(z) = u_0(z) + \eta$ and $v(z) = v_0(z) + \eta$, where u_0 and v_0 are the unperturbed G2S wind profiles and η is the noise vector. Figure 2 illustrates the addition of noise by comparing zonal and meridional winds with and without Gaussian noise with a standard deviation of 5 m/s.

A comparison between the observations and predictions, for different levels of added noise, is shown in Figure 3. Gaussian noise with σ equal to 5 m/s, 10 m/s, and 20 m/s have been added to the unperturbed wind profiles in Figure 2. The uncertainties used are within the approximate range of estimated uncertainties in G2S models (Drob et al., 2010), although the variation in uncertainty with height is not accounted for here. The predictions estimated here do not include direct arrivals -- only ducted arrivals are considered. Furthermore, multiple bounces are not considered in this study, eliminating the added complexity of accounting for topography (Arrowsmith et al., 2007). Multiple atmospheric realizations have been computed at each noise level, with similar ray-tracing results obtained each time. The results

presented below correspond to single realizations, but these are broadly representative of multiple runs in terms of the highlighted regions where predictions match (see Figure 3).

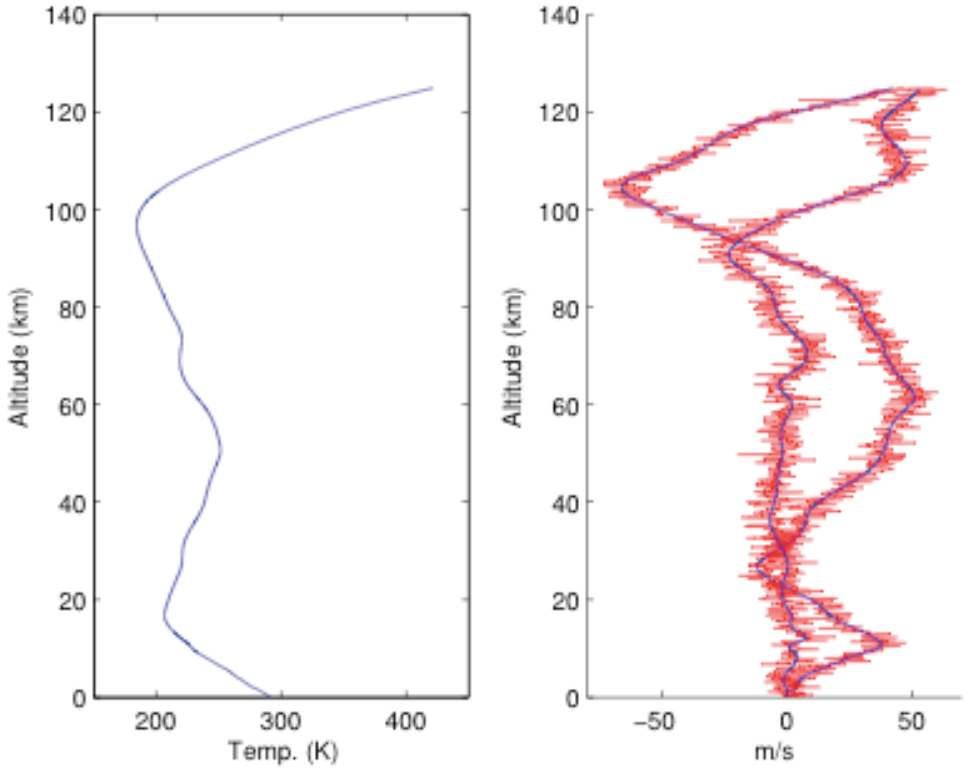

Figure 2. Profiles of the 1D temperature (left panel) and winds (right panel) extracted from the G2S model for 19:00 on 11/01/2007 at the test location. Unperturbed zonal and meridional winds are represented by blue lines, while perturbed wind profiles (using $\sigma = 5$ m/s) are shown in red.

The predicted bounce-points (locations where rays are predicted to hit the ground), which are shown in Figure 3, assume an omni-directional source and do not account for the known source directivity. The bounce-points were predicted by shooting a suite of rays at azimuths of 0–355°, and launch angles of 0–90°, with 5° spacing in both azimuth and launch angle. With no added noise, the geographic distribution of bounce-points reflects the strong positive zonal wind in the stratosphere, common at this latitude during the winter months, which enhances the stratospheric duct to the east and destroys the stratospheric duct to the west (noting that stratospheric group velocities are typically 0.28 km/s–0.31 km/s).

The results shown in Figure 3 highlight that, although some arrivals are not predicted using the unperturbed G2S profiles, they can be predicted when noise is added to the profiles. For example, observations with v_g = 0.28 km/s to the southwest of the test are only predicted with σ = 5-10 m/s; observations with v_g < 0.27 to the northeast of the test are only predicted with σ = 20 m/s. As would be expected, with increasing noise, returns are predicted at ever-closer distances. However, due to the strong zonal winds that favor propagation to the east, few returns are predicted towards the west at these noise levels, with the exception of thermospheric returns.

The full suite of observations can only be explained through the combination of simulations with varying noise levels. This detail is important because it implies that, for phase identification (and thus also for location purposes), a probabilistic approach is necessary. For example, an observed arrival may be explained as either a stratospheric, or tropospheric, arrival depending on the standard deviation of the wind perturbation addition.

Our contention is that if we can reliably predict arrivals through the addition of noise to atmospheric wind models, the simple uniform prior of Modrak et al. (2010) may be refined using a stochastic prediction model. By the principle of reciprocity, the Tau-P equations can be calculated from the receiver perspective by integrating the ray equations with a negative time step. Thus, by tying the standard deviation of wind perturbations to probability (where more probable predictions are based on smaller standard deviations of additive noise), we can develop a non-uniform prior PDF, for a given signal backazimuth and arrival time, based on Tau-P predictions. In effect, we can directly relate celerity to the standard deviation of wind perturbations, and subsequently relate wind noise probabilities to group velocity probabilities. Further research is needed to develop this R&D concept, implementing prediction model simulations into BISL2.0.

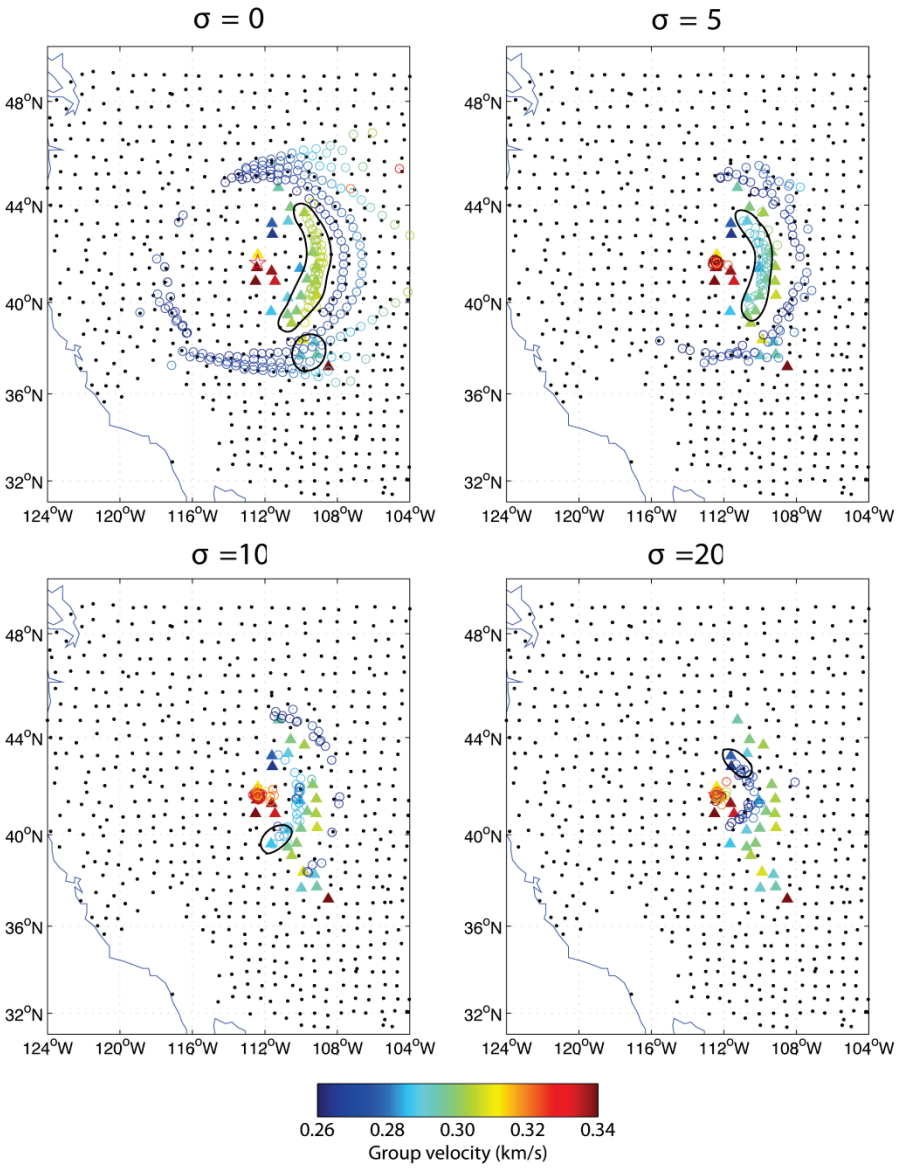

Figure 3. Plots comparing predictions (open circles) and observations (filled triangles) for different levels of noise added to the atmospheric data. Black dots represent stations that did not record the test. The predictions and observations are plotted on the same color scale, which represents group velocity. Thermospheric predictions have been removed for clarity. Observations enclosed by black lines are uniquely predicted for that given noise level.

Experimental Characterization of Seasonal Variations in Infrasonic Travel Times in the Korean Peninsula with Implications for Infrasound Location

The purpose of this component of our work is to experimentally characterize infrasonic travel time and construct quantitative celerity models that depend on the season and propagation path. In support of this deterministic approach to travel-time assessment we collected nearly daily repetitive infrasonic observations over a two-year time period from ground-truth events at an active mine. These events included more than 1,000 surface blasts that occurred daily, with multiple events on active days, over the 2 years. Variations in infrasound propagation based on the data are quantified at the two infrasound arrays CHNAR and ULDAR in Korea (Figure 4), both located at similar distances from the mine but with different propagation environments - one path dominated by the continent and the other by the ocean.

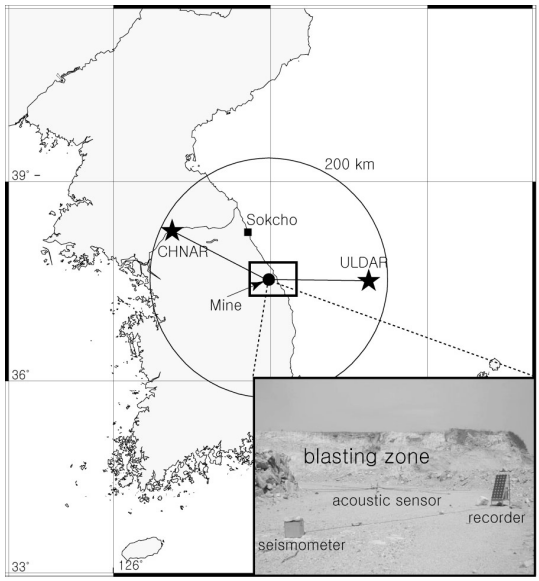

Figure 4. Locations of the open-pit mine (circle), two infrasound arrays (stars) and weather balloon station (square) used in this study. A photograph of one in-mine seismo-acoustic station is shown in the lower right.

Array processing based on the progressive multi-channel correlation (PMCC) (Cansi, 1995), is used to detect and analyze the blast-associated infrasonic signals and to construct a celerity model for each path. Characteristics of the two sets of experimental celerity models include seasonal dependent path effects to each array. Ray tracing using long-term atmospheric models supplemented by shallow atmosphere constraints provided by weather balloon data was performed for comparison with the observations.

Variations of infrasound propagation. During the two years of in-mine sensor operation, 1,066 blasts were detonated, more than one blast per day on average. 97% of the blasts occurred at or around 03 UTC (12 pm local time). The origin time and approximate location of each event was estimated using the seismic and infrasound observations from the in-mine stations. Infrasonic array data were analyzed using the PMCC method, in order to detect blast-associated infrasonic signals. The wave parameters of each detected signal, including the arrival time and azimuth, were then estimated at each array. Figure 5 displays the waveforms and analysis results for one set of the ground-truth events. The left figure shows near-field seismic and acoustic signals recorded at the two in-mine stations (ACE3 and ACE7). The acoustic signals in this case were clipped due to instrument dynamic range and the close distance to the 10-ton blast. We simply used the center of the main blasting zone as a source location for all blasts. PMCC results are also shown in the figure. WinPMCC v2.1 was used to make the regional wavefield estimates focusing on a phase velocity range of 0.25-0.40 km/s using a window length 20 s, and a frequency band 0.5–5 Hz. After signal association, we compiled travel times and wave parameters determined from PMCC.

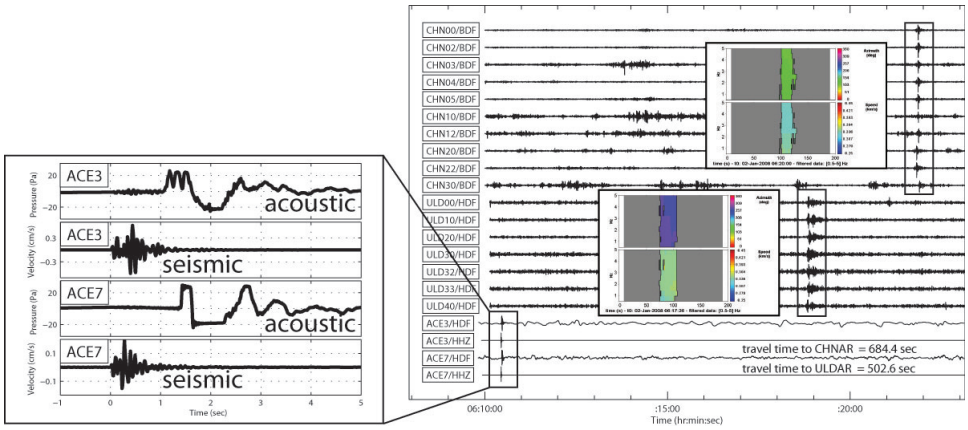

Figure 5. Example data for a blast charged with 10 tons of explosives. (left) The four waveforms from the blast are the near-field seismic and acoustic signals recorded in the mine. (right) Boxes mark the blast-associated infrasound signals recorded at the two regional arrays with the upper ten waveforms from CHNAR, excluding one bad channel (CHN32), and next seven waveforms from ULDAR. The corresponding PMCC results display the estimates of azimuth (upper) and apparent velocity (lower) for the detected signals. Measured travel times for both infrasonic signals are listed in the lower right.

Figure 6 documents the variation of infrasound travel times and azimuths to the two arrays for all the ground-truth events that were observed over the 2 years. Despite similar propagation distances, the average travel times were significantly different to the two arrays, with arrivals at ULDAR on average 150 seconds earlier than those at CHNAR. For CHNAR, the celerities calculated from the distances and travel times ranged from 260 to 289 m/s, which corresponds to the characteristic value of stratospheric returns (Evers and Haak, 2007).

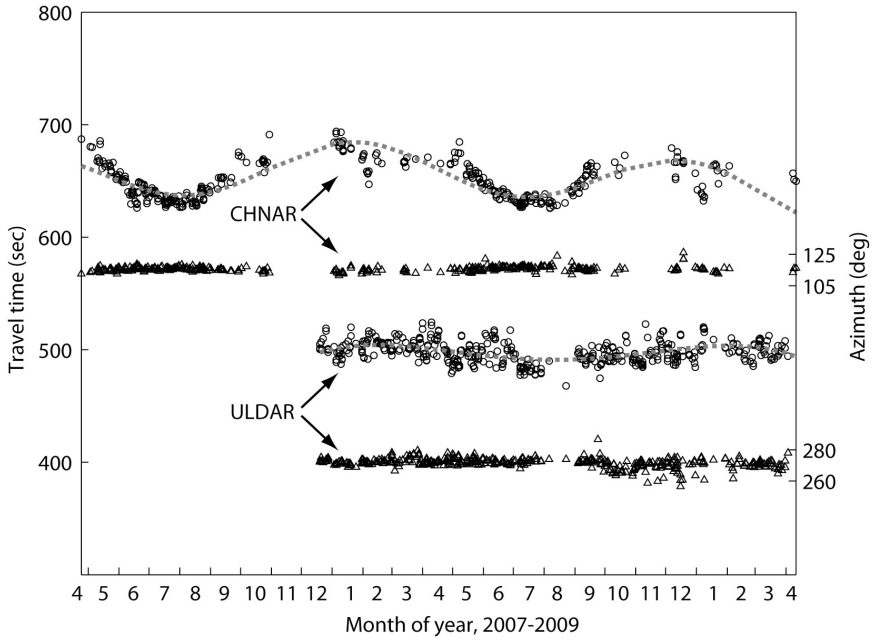

Figure 6. Variations of travel times (circles) and azimuths (triangles) estimated at both arrays from the ground-truth events recorded over the 2 years of the study. The dotted lines superimposed on the observed travel times are sinusoidal celerity models that were fit to the observations. Note that ULDAR was installed in December 2007 and so there is a shorter time period of observation.

In addition, the travel times showed systematic seasonal variations with signals arriving up to 68 seconds faster in the summer. Thus, the celerity showed a smoothly varying cyclical change with time, with

velocities of ~0.26, ~0.29, and ~0.27 km/s in the winter–spring, summer, and fall seasons, respectively. This systematic variation in observed celerity is consistent with the contention that the travel times of infrasound signals are strongly dependent on the seasonal ambient sound speed along the path. In contrast, the infrasound signals arriving at ULDAR showed relatively large celerities (322 to 361 m/s), characteristic of tropospheric returns. The travel times to ULDAR show little seasonal variation but document larger daily variations of up to 56 second in the travel times between days. These observations can be partially attributed to the dominant effect of the ocean on temperatures at the ocean–atmosphere boundary.

Path variations also impact the ability to detect the arrivals. Signals at CHNAR were most likely to be detected in the summer. Many signals were not detected during the fall–winter–spring seasons, even though strong source signals were identified at the in-mine stations for these times. Detection at ULDAR was low in summer (August) but stable during the other seasons. Thus, the seasonal detection at the two arrays was complementary, as shown in Figure 6 as result of the azimuthal differences of the two arrays relative to the mine. This variation in detection can be partially explained by seasonal changes in the atmospheric wave duct attributable to known seasonal wind in and around the Korean Peninsula with winds northwesterly in the winter and southeasterly in the summer. In contrast to the variation of travel times, the azimuth estimates showed little variation with season at either array (Figure 7). The mean and variance of the azimuth estimates were 115.6±1.6^{o} at CHNAR (115.8^{o} of true azimuth) and 271.5±3.1^{o} at ULDAR (271.7^{o}), respectively. The insensitivity of backazimuth to seasonal variations is consistent with the relatively weak meridional winds (5.9% and 27.2% of annual average zonal wind speed at 10 and 30 km above the mine, respectively, estimated from Horizontal Wind Models (Drob et al., 2008) in the region, which are normal to the dominantly EW propagation paths in this study.

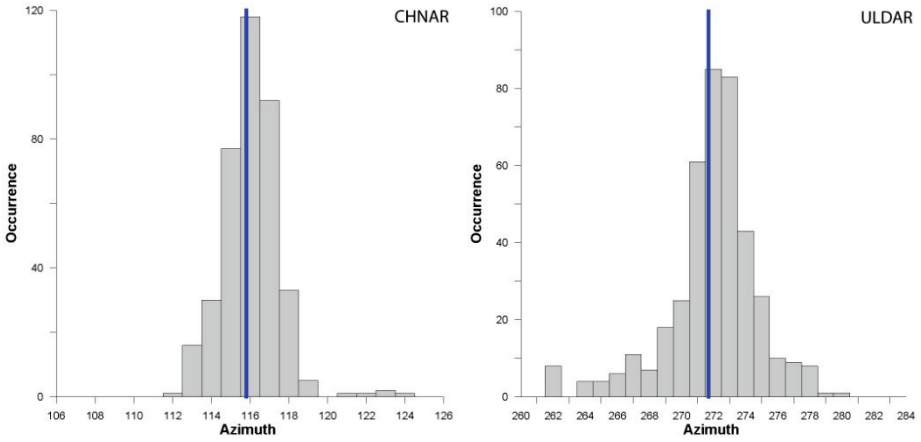

Figure 7. Distribution of backazimuth estimates at CHNAR (left) and ULDAR (right) for all the ground truth events observed at the two arrays. The blue line represents the true backazimuth to the mine where the events occurred.

Modeling of Infrasonic Propagation. Atmospheric ray tracing was performed for all the observations over the 2 years of the study using a combination of empirical atmospheric models (Horizontal Wind Model/Mass Spectrometer, Incoherent Scatter: HWM07 (Drob et al., 2008)/MSISE-90 (Hedin et al., 1991) for the upper atmosphere and weather balloon data for the lower atmosphere. The lower part of the effective sound velocity profiles (ESVP) used for ray tracing (Hagerty et al., 2002) was based on the weather balloon data from the Sokcho station, which is closer to both the mine and arrays than other stations operated by the KMA. The measurement height of the balloon data depended on the day, but data were usually available to an approximate altitude of 30 km and included temperature, wind direction, and wind speed. Data acquired at 00 UTC was used for the modeling because it is within 3 hours of the average time of the blasts. Ray tracings at a 0.1^{o} intervals were computed for each day of the experimental period and included models for 726 days at CHNAR and 484 days at ULDAR (smaller number of days for ULDAR reflects its more recent installation, December 2007). When trajectories of a ray passed within 1 km (capture radius) of the array, the ray was identified as an eigenray for the infrasonic phase. Of the eigenrays computed on a given day, the ray with highest turning height was selected as a representative

eigenray for the day. In case of CHNAR, the total rays from the simulations were grouped into four dominant classes: (1) in 43.8% of the cases there exists a thermospheric phase but CHNAR is located in a acoustic shadow zone for the rays, *It_shadow*; (2) in 36.9% of the cases there exists a stratospheric phase but CHNAR is again located in a shadow zone, *Is_shadow*; (3) in 16.7% of the cases there was a tropospheric phase that was predicted to return to CHNAR, *Iw_eigen*; and (4) in 2.6% of the cases there was predicted a stratospheric phase that is predictable to return to CHNAR, *Is_eigen* . In case of ULDAR, four dominant cases were identified and included *It_shadow* (9.9%), *Is_shadow* (5.4%), *Iw_shadow* (3.1%), and *Iw_eigen* (81.6%). Unlike the other shadowing phase, the *Iw_shadow* phases jumped ULDAR with bounces at the surface.

Figure 8 displays the variation of ESVP for the 2 years of the study along with the ray-tracing results. The refraction altitudes of each daily eigenray from the mine to the individual arrays are superimposed on the ESVP.

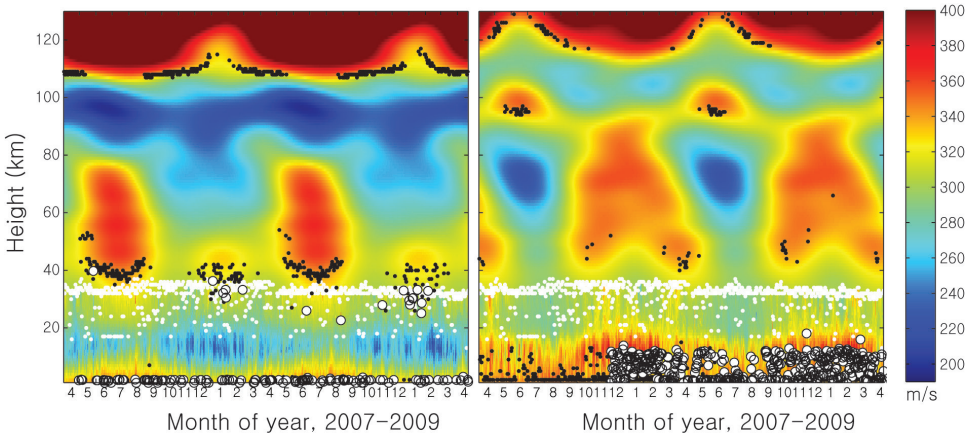

Figure 8. Ray tracing results using effective sound velocity profiles (ESVP) for the path from the mine to CHNAR (left) and to ULDAR (right) for the 2 years of the study. White dots indicate boundary heights between balloon data and the empirical data used for the ray tracing. Black dots indicate the lowest possible refraction heights where the sound speed is larger than that at source. White circles indicate turning points in the atmosphere from the predicted eigenrays for each day at 00 UTC.

For CHNAR, ray tracing predicted a smaller number of eigenrays representative of stratospheric returns than that documented in Figure 6. Although many stratospheric returns were predicted from ray tracing (the black dots around 40 km altitude), CHNAR was in the so-called zone of silence in most of these prediction. This comparison implies that the ESVP, particularly the empirical models with stratospheric returns, were not sufficient to predict the real observations or that the capture radius was too small, even though the predictions for the *Is_eigen* are increased by widening the capture radius, for example 4.7% for 5 km and 14.5% for 10 km of capture radius. Most *Is_eigen* phases at CHNAR were predicted during the winter (see January of 2008 and 2009) with refraction altitudes corresponding to heights sampled by the balloon data. These predictions can be explained by not only the slow sound speed at the ground but also the slightly higher velocity channel at stratospheric heights during this season. The higher level of signal detection predicted for the mid-winter (January) in comparison to the spring and fall seasons was consistent with the observations detailed in Figure 6. The calculations also predicted many *Iw_eigen* phases that refracted at very low altitudes and experienced bounces at the ground surface but the corresponding phases were not clearly observed in the ground truth data. This second result suggests that the *Iw* phase may have limited horizontal propagation along the continental path which includes significant topographic variation between the mine and CHNAR. In contrast, many eigenrays returned to ULDAR by refraction at altitudes lower than 20 km. These altitudes were in the range where the balloon data were collected.

Infrasound Location of Ground Truth Events. Infrasonic signals from 130 blasts were detected by both arrays. In this study, we calculated two different location sets for these selected blasts. The first set of location estimates were determined by assuming common stratospheric phase for both arrays with constant celerity of 0.3 km/s for all seasons in the least-square method. The second set of location estimates were

calculated using simple sinusoidal celerity model which were fit to the observation (dotted lines in Figure 6), and includes seasonal dependences as described. The location results are summarized in Figure 9 with the blue squares representing the first set of locations and the red ones the second location set using the seasonal dependent celerity models. 95% confidence ellipses for each location set are also included in the figure. The centroid for the location of the first set is biased about 17.8 km to the east of the mine due to the discrepancies between the assumed constant celerity and observed celerities shown in Figure 6. The average location estimates using the experimentally determined celerity models that included seasonal path effects showed only a 1.7 km offset from the mine location. This result suggests that, for infrasonic source location at regional distances, the dependence of infrasound propagations on seasons and path environments should be quantified and its effects incorporated into the infrasound location method in order to produce improved location estimates. In the figure, black circles indicate seismic locations for the blasts extracted from the seismological catalog of the KEMS. Of the total ground truth dataset used in this study, the KEMS detected 589 events (open circles) with local magnitude ranging from 0.5 to 1.8 M_L. Yellow circles in the figure indicate the 100 seismic locations which correspond to the 130 blasts located using only the infrasound signals as described above. It is interesting to note that there were 30 events in the infrasound set that did not produce seismic events in the database. Comparing the infrasonic location with the seismic location, suggests that the infrasonic location including seasonal path effects are at least comparable to seismic location in case of small-magnitude surface explosions at regional distances.

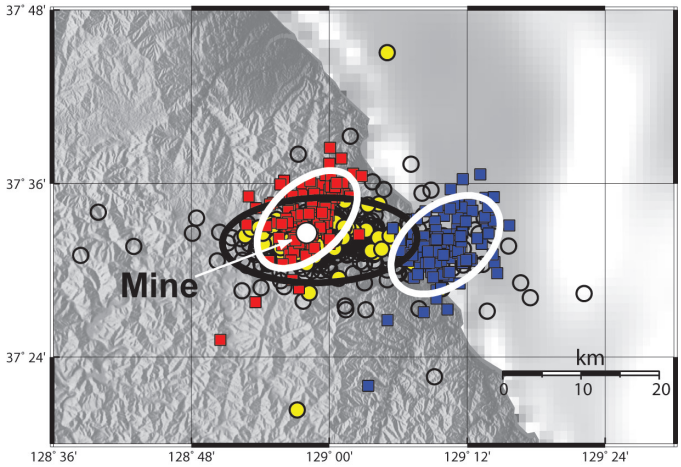

Figure 9. Two infrasonic locations results for selected ground truth events using constant celerity model (blue squares) and sinusoidal model (red squares). Circles indicate seismic locations of the ground truth events determined by the KEMS.

CONCLUSIONS AND RECOMMENDATIONS

The stochastic study suggests that one can reliably predict arrivals through the addition of noise to atmospheric wind models. The implication is that the simple uniform prior of Modrak et al. (2010) may be refined using a stochastic prediction model. By the principle of reciprocity, the Tau-P equations can be calculated from the receiver perspective by integrating the ray equations with a negative time step. Thus, by tying the standard deviation of wind perturbations to probability (where more probable predictions are based on smaller standard deviations of additive noise), we can develop a non-uniform prior PDF, for a given signal backazimuth and arrival time, based on Tau-P predictions. In effect, we can directly relate celerity to the standard deviation of wind perturbations, and subsequently relate wind noise probabilities to group velocity probabilities.

The complementary two-year deterministic study of infrasound wave propagation has utilized ground truth events collected at an active mine in Korea. The dataset included 1,066 blasts and highlights the variation of infrasonic propagation due to the seasonal variation of atmospheric structures and propagation path environments. The blast-associated infrasonic signals were analyzed at two distant infrasound arrays, which

were located at similar distances (zone of silence) from the mine but pointed in different azimuth directions over different path environments (continental and open ocean). Infrasonic waves traveling NW toward CHNAR over the continent propagated as guided waves between the ground and stratosphere, with a characteristic celerity range of 260–289 m/s. These observations documented seasonal cyclical variations in travel time. The infrasonic waves traveling E to ULDAR also propagated as guided waves, but observed celerities indicated that wave ducts were formed at relatively low heights in the troposphere. The celerity range was correspondingly large (322–361 m/s), even though the propagation distances to both arrays were similar. ULDAR showed more daily variation in travel time than seasonal variation. The lower refractions were compared and verified by ray tracings with balloon data constraining the lower atmosphere. In particular, the observations at ULDAR support the existence of an ephemeral 'SOFAR' layer in the atmosphere (Herrin et al., 2006) throughout the year over the open ocean. Finally, the dataset illustrates that a celerity model that captures the seasonal path effects can substantially improve infrasound location procedures. The infrasound only location resulted in improved locations when compared routine seismic locations for these small-magnitude surface explosions observed at regional distances.

ACKNOWLEDGEMENTS

We would like to thank Mr. Kwan Kyo Chung, section manager of the mine office for his thoughtful supports during the experiment. We used atmospheric data collected by the Korea Meteorological Administration (www.kma.go.kr). This work was also supported by the Basic Research Project of the Korea Institute of Geoscience and Mineral Resources funded by the Ministry of Knowledge Economy of Korea.

REFERENCES

Arrowsmith, S. J., D. Drob, M. A. H. Hedlin, and W. Edwards (2007). A joint seismic and acoustic study of the Washington State bolide, *J. Geophys. Res*., 112, doi:10.1029/2006JD008001.

Cansi, Y. (1995). An automatic seismic event processing for detection and location: the PMCC method, *Geophys. Res. Lett.* 22: 1021–1024.

de Groot-Hedlin, C. D., M. A. H. Hedlin, and K. T. Walker (2008). Evaluation of infrasound signals from the shuttle Atlantis using a large seismic network, *J. Acoust. Soc. Am*. 124: 1442–1451, doi:10.1121/1.2956475.

Drob, D. P., et al. (2008). An empirical model of the Earth's horizontal wind fields: HWM07, *J. Geophys. Res*. 113: A12304, doi:10.1029/2008JA013668.

Drob, D., Garcés, M., Hedlin, M., and Brachet, N. (2010). The temporal morphology of infrasound propagation. *Pure Appl. Geophys.* 167: 437–453.

Evers, L. G., and H. W. Haak (2007b). Infrasonic forerunners: Exceptionally fast acoustic phases, *Geophys. Res. Lett*. 34: L10806, doi:10.1029/2007GL029353.

Evers, L. G. (2009). Imaging of the atmosphere with infrasound, *Proceedings of Internoise, 2009,* Ottawa, Canada, August 23-26, 2009.

Garces, M. A., Hansen, R. A., and Lindquist, K. G. (1998). Traveltimes for infrasonic waves propagating in a stratified atmosphere, *Geophys. J. Int.* 135: 255–263.

Gardner, C. (1993). Gravity Wave Models for the Horizontal Wave Number Spectra of Atmospheric Velocity and Density Fluctuations, *JGR* 98; D1, 1035–1049.

Gibson, R .G., Drob, D. P., and Broutman, D. (2009). Advancement of Techniques for Modeling the Effects of Fine-Scale Atmospheric Inhomogeneities on Infrasound Propagation, in *Proceedings of the 2009 Monitoring Research Review*: *Ground-Based Nuclear Explosion Technologies*, LA-UR-09-05276, Vol. 2, pp. 714–723.

Hagerty, M. T., W. Y. Kim, and P. Martysevich (2002). Infrasound detection of large mining blasts in Kazakstan, *Pure Appl. Geophys*., 159: 1063–1079.

Hedin, A. E. (1991). Extension of the MSIS thermosphere model into the middle and lower atmosphere, *J. Geophys. Res*., 96(A2), 1159–1172.

Herrin, E. T., T. S. Kim, and B. W. Stump (2006). Evidence for an infrasound waveguide, *Geophys. Res. Lett*. 33: L07815, doi:10.1029/2005GL025491.

Modrak, R. T., S. J. Arrowsmith, and D. N. Anderson (2010). A Bayesian framework for infrasound location, *Geophys. J. Int*., 181: doi:10.1111/j.1365-246X.2010.04499.x

Whitaker, R. W. and Norris, D. E. (2008). Infrasound Propagation, in *Handbook of Signal Processing in Acoustics*, Springer, New York.